JMEPEG (2008) 17:363–368
DOI: 10.1007/s11665-008-9214-8

1059-9495/$19.00

Modeling of Transformation Superplastic Forming of Ti Alloys

Qizhen Li

(Submitted November 8, 2007; in revised form February 5, 2008)

Transformation superplastic forming is an attractive alternative forming technique to microstructural superplastic forming, since it requires no special microstructures and, therefore, eliminates the limitation of superplastic forming capability to only expensive materials with stable high-temperature fine grains. Transformation superplasticity occurs through biasing the internal stress produced from an allotropic phase transformation by a small external stress. In this work, finite element modeling was implemented to study the transformation superplastic forming of domes from flat circular thin plate samples. The evolution and distribution of stress, strain, and dome thickness was analyzed in detail. The thickness distributions in the formed domes were compared with the theoretical predictions of two models, which assume different stress states in the domes. The appropriate stress state was identified through this comparison. Different gas pressure amplitudes were applied during forming to investigate the effect on the formed-dome apex height, when the forming time was fixed.

Keywords mechanical testing, shaping, titanium

1. Introduction

Superplastic forming is broadly used in a wide variety of industries, due to the corresponding advantages like near-net shape forming of complex shapes, reduction of part count, minimization of scrap rates, cost/weight savings, etc. There are two fundamental types of superplasticity of materials, i.e., microstructural superplasticity and transformation superplasticity (Ref 1). The microstructural superplasticity mechanism is the fundamental mechanism for most parts manufactured by superplastic forming, which requires equiaxed grains of less than 10 μm and grain stability at elevated temperatures. The special microstructure is generally furnished by complex thermomechanical processing. Extensive research effort on superplasticity was performed to understand the basic mechanisms of superplasticity, develop superplastic properties in known commercial materials through thermomechanical processing, and develop new materials with superplasticity (Ref 2-15). Ultrafine-grained materials were produced by severe plastic deformation methods to increase the forming strain rate (Ref 2-4, 15). Nanostructured materials were also developed and characterized for superplasticity (Ref 7-14). On the contrary, transformation superplasticity has no requirements on the microstructure of materials, which eliminates some intermediate processing procedures and reduces cost. Transformation superplasticity requires the existence of an internal stress/strain during the process. Some small biasing external stress is applied to realize the net deformation. The sources of the internal stress can be polymorphic solid phase transformations, differences in the coefficients of thermal expansion, etc. (Ref 16-22). Detailed knowledge about transformation superplastic forming is needed, and a dome-forming test (Ref 22, 23) can be used to understand the forming process. In this work, superplastic forming simulations are based on the $\alpha \leftrightarrow \beta$ solid phase transformation when the temperature cycles around the β-transus of Ti-6Al-4V. The great benefit of modeling is that (1) the detailed dimensions/shapes of the dome are available for each moment of the forming process, and (2) the time and cost is largely reduced compared to corresponding experimental investigations. Section 2 describes the computational and theoretical fundamentals. Section 3 reports and analyzes the results on the stress, strain, and thickness distribution within the formed dome, the dome thickness evolution with the forming time, and the relation between the dome apex height and the applied forming gas pressure.

This article was presented at Materials Science & Technology 2007, Automotive and Ground Vehicles symposium held September 16-20, 2007, in Detroit, MI.

Qizhen Li, Chemical and Metallurgical Engineering, University of Nevada, Reno, NV 89557. Contact e-mail: qizhenl@unr.edu.

2. Model and Theory Description

Finite element modeling was used to study the dome forming of Ti-6Al-4V through the transformation superplastic forming technique. The sample prior to forming simulation was a flat circular plate of 62 mm diameter and 1.5 mm thickness. The sample experienced the repeating 8-min temperature cycles around the β-transus (~995 °C for Ti-6Al-4V (Ref 24)). Each cycle was composed of a 4-min heating from 840 °C to 1030 °C and 4-min cooling from 1030 °C to 840 °C as shown in Fig. 1. A biasing external stress was provided by the forming gas pressure to realize the net nonzero deformation. Modeling was performed using the commercial finite element software ABAQUS with a linear-brick-element C3D8R. The following

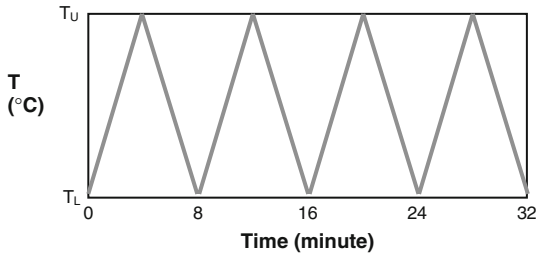

Fig. 1 The temperature profile of thermal cycles with the upper and lower temperatures of T_U and T_L, respectively. Here, T_U = 1030 °C and T_L = 840 °C for Ti-6Al-4V. Each cycle is 8 min, and includes a 4-min heating from 840 °C to 1030 °C and 4-min cooling from 1030 °C to 840 °C

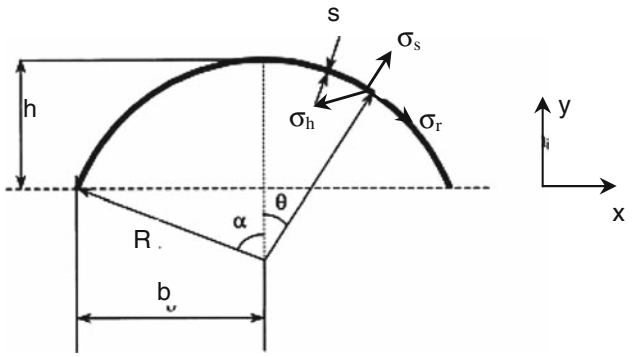

Fig. 2 A sketch of the cross section of a dome along the plane through the dome apex with the geometry information

Eq 1 provided the constitutive relation employed. The boundary and load conditions were defined as a fixed circumference of the plate sample with the gas pressure, P, on one side of the circular surface. The formed dome geometry was accurately approximated as a spherical cap with its cross section at the apex schematically depicted in Fig. 2. R, h, and α are the radius, height, and half of the span angle of the spherical cap, respectively. S is the thickness of the dome, which varies with position. θ is the angle between the radius through the apex and the radius through a position on the dome. The applied pressure was fixed during the doming process, which generated the biasing external applied stress in the dome sample.

During transformation superplastic forming, a small pressure is used to generate a small stress. Deformation is dominated by transformation superplasticity, and the contribution from creep is neglected. A large amount of research (Ref 16, 20-23) showed the linear relationship between the transformation superplastic strain rate $\dot{\varepsilon}_{TSP}$ and the effective applied stress (von Mises stress) $\sigma_{von\ Mises}$

$$\dot{\varepsilon}_{TSP} = K_{TSP} \cdot \sigma_{von\ Mises} \quad \text{(Eq 1)}$$

where K_{TSP} is the transformation superplastic coefficient (Ref 22).

The three principal stress components from the applied pressure are represented in Fig. 2 as the radial stress σ_r, the hoop stress σ_h, and the thickness stress σ_s. Since the thickness of the dome is thin and one dome surface is traction-free, the thickness stress can be neglected in the analysis. According to the thin shell theory (Ref 25, 26), the radial stress σ_r at any position of the dome is

$$\sigma_r = \frac{PR}{2S} \quad \text{(Eq 2)}$$

where P is the applied gas pressure, R is the radius of the dome, and S is the thickness of the dome at the corresponding location. At the dome apex, the stress is in a balanced biaxial state due to the symmetry, and the hoop stress σ_h is

$$\sigma_h = \sigma_r \quad \text{(Eq 3)}$$

At the dome edge, a plane strain state exists and $\varepsilon_h = 0$. The stress and strain components are σ_r, σ_h, ε_r, ε_h, and ε_s. The constraints from the boundary condition and the compatibility are

$$\varepsilon_h = 0 = \frac{\sigma_h}{E} - \frac{\nu\sigma_r}{E} \quad \text{(Eq 4)}$$

$$\varepsilon_r = -\varepsilon_s = \frac{\sigma_r}{E} - \frac{\nu\sigma_h}{E} = \frac{\nu\sigma_r}{E} + \frac{\nu\sigma_h}{E} \quad \text{(Eq 5)}$$

where E and ν are the Young's modulus and Poisson's ratio of the dome material. Solving Eq 4 and 5, the hoop stress σ_h at the dome edge is

$$\sigma_h = \frac{\sigma_r}{2} \quad \text{(Eq 6)}$$

The effective stress is

$$\sigma_{von\ Mises} = \sqrt{\frac{(\sigma_r - \sigma_h)^2 + (\sigma_r - \sigma_s)^2 + (\sigma_s - \sigma_h)^2}{2}} \quad \text{(Eq 7)}$$

There are two theoretical models to predict thickness distribution of the final dome. The first model was developed by Enikeev and Kruglov (Ref 27) and assumed that each meridian passing through the dome apex is representative of the doming deformation and the stress state appropriately varies from balanced biaxial at the apex to plane strain at the dome periphery. The predicted dome thickness S varies across the dome according to the following equation

$$S = S_0 \cdot \left(\frac{\sin\alpha}{\alpha}\right)^2 \cdot \frac{\theta}{\sin\theta} \quad \text{(Eq 8)}$$

where α is the angle subtended by the radius line through the apex and that through the edge of the dome (thus describing the dome radius of curvature), and the position is expressed by the angle θ, which varies between $\theta = 0$ at the dome apex and $\theta = \alpha$ at the dome periphery. S_0 is the initial plate thickness. The other thickness-distribution model by Ragab (Ref 28) assumes a balanced biaxial stress state throughout the dome, and the thickness for any point on the dome is

$$S = S_0 \cdot \left(\frac{\cos\alpha + 1}{\cos\theta + 1}\right)^2 \quad \text{(Eq 9)}$$

3. Results and Discussion

Different cases were modeled in this work. The stress, strain, and dome thickness distributions in the formed dome are

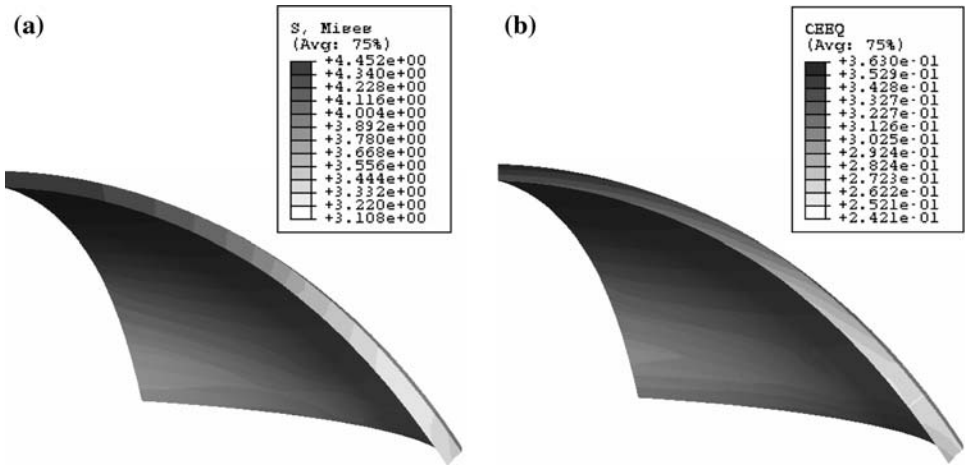

Fig. 3 The von Mises stress and equivalent creep strain distributions in the dome formed under the pressure of 250 kPa for thirty-two 8-min cycles (256 min or 15.36 ks). (a) von Mises stress distribution; (b) equivalent strain distribution

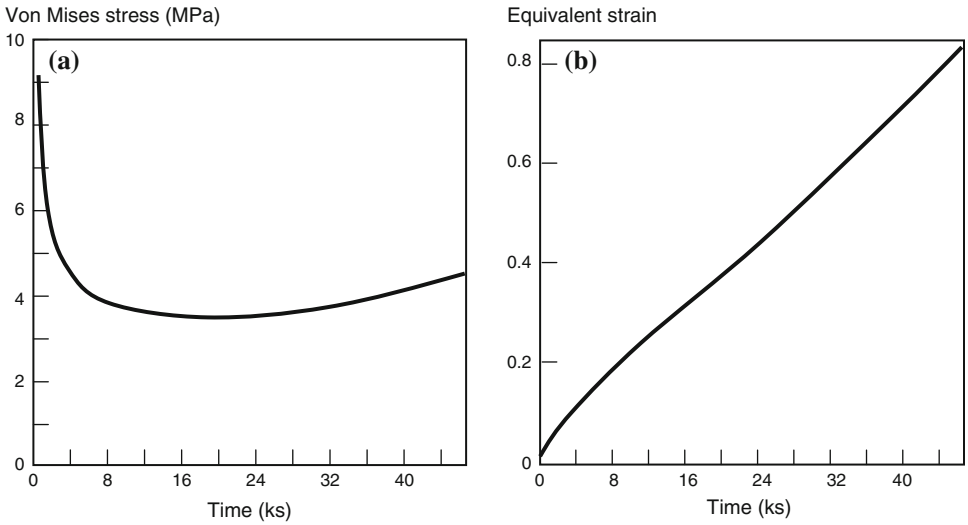

Fig. 4 The von Mises stress and equivalent creep strain at the dome apex in the dome formed under the pressure of 200 kPa for ninety-eight 8-min cycles (784 min or 47.04 ks). (a) von Mises stress; (b) equivalent strain

reported. The dome thickness evolution with forming time was obtained for different locations in the dome. A series of gas pressures was used to study the relation between the dome apex height and applied pressure.

3.1 Stress and Strain Distributions

To take the advantage of symmetry, a quarter of the plate was simulated. Figure 3 illustrates the distribution of von Mises stress and equivalent strain within the dome formed after thirty-two 8-min cycles under the pressure of 250 kPa. The effective stress ranged from 3 to 4.5 MPa, and the equivalent strain ranged from 0.24 to 0.36. The maximum stress and strain were located at the dome apex. The stress and strain decreased when moving from the apex to the edge of the dome.

The evolution of effective stress and strain at the dome apex is shown in Fig. 4 for a dome formed after ninety-eight 8-min cycles under the pressure of 200 kPa. According to Eq 2, the radius stress increased with the increase of R and the decrease of S when the applied pressure P was fixed. At the beginning of the deformation, the sample was flat and R was infinity, which led to an infinite applied stress as shown in Fig. 4(a). The stress quickly decreased and remained more or less constant around 4 MPa during the forming process. Based on Eq 2, the effect of the decrease of both the dome radius and the dome thickness cancels out and results in the stable stress magnitude. The equivalent strain increased almost linearly with forming time as shown in Fig. 4(b). The final equivalent strain at the formed dome apex was about 84%.

3.2 Thickness Evolution

Figure 5 and 6 show the thickness evolution with the forming time for the doming tests under the pressure of 250 and 200 kPa, respectively. Six positions were chosen from the dome to display the evolution for both cases. Position 1 is at the apex, position 6 is close to the edge, and the other positions are in between. For all positions, the thickness decreased with

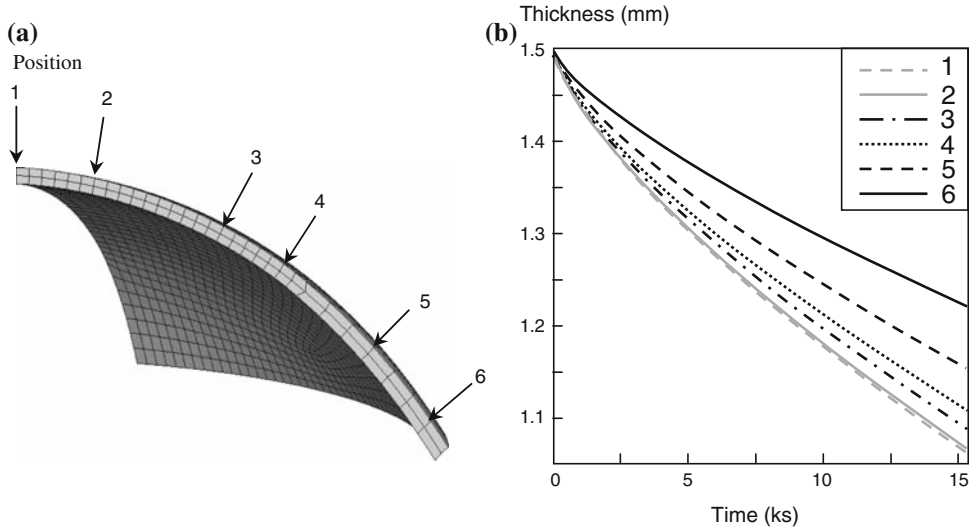

Fig. 5 The thickness evolution with the forming time at the six chosen positions for the case with the gas pressure of 250 kPa. (a) The six locations studied; (b) the thickness evolution at the six locations

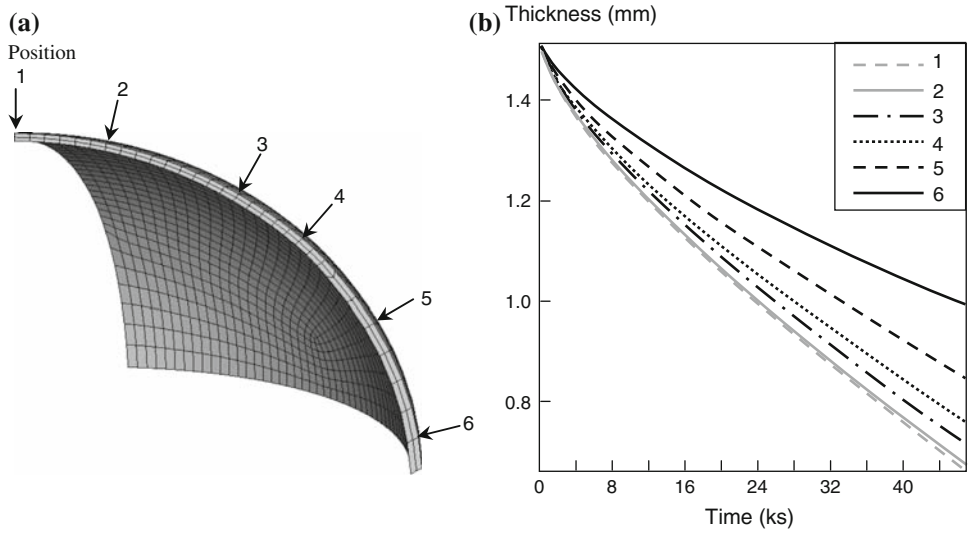

Fig. 6 The thickness evolution with the forming time at the six chosen positions for the case with the gas pressure of 200 kPa. (a) The six locations studied; (b) the thickness evolution at the six locations

forming time. The apex thickness was thinnest, the edge thickness was thickest, and the thickness increased from the apex position to the edge position for all forming times. When the forming time was fixed, the thickness decreased faster for the case with a higher applied gas pressure.

3.3 Thickness Distribution

The dome thickness was obtained at different locations from the apex to the edge for the formed domes. Results show the relation between S/S_0 and the position distance from the apex along the x direction in Fig. 2, where S is the current thickness and S_0 is the initial thickness. Figure 7 provides the results for the dome formed after 32 8-min cycles under the pressure of 250 kPa. The theoretical predictions were also calculated for the two models described in Section 2. In order to generate the theoretical predictions, the spherical cap radius, R, and the angle, α, were computed first based on the information of the apex height, h_{apex}.

$$\alpha = \pi - 2\text{atan}(b/h_{\text{apex}}) \quad \text{(Eq 10)}$$

$$R = b/\sin(\alpha) \quad \text{(Eq 11)}$$

The apex height, h_{apex}, the angle, α, and the radius, R, for this case were 15.9 mm, 0.975 rad, and 36.3 mm, respectively. Figure 8 provides the results for the dome formed after ninety-eight 8-min cycles under the pressure of 200 kPa. The corresponding h_{apex}, α, and R were 27.5 mm, 1.45 rad, and 41.4 mm, respectively. The results show that the Enikeev and Kruglov model matches the simulation results very well for both cases, while the Ragab model predictions deviate significantly from the modeling results. Thus, the results indicate

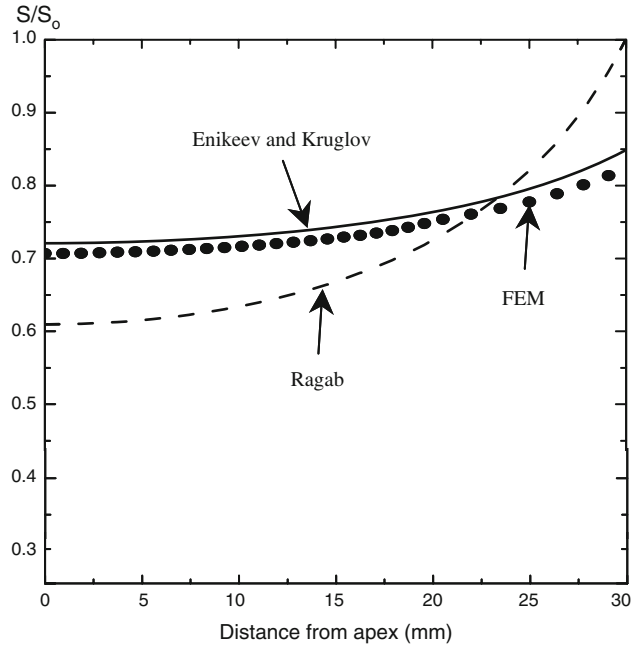

Fig. 7 The dome thickness distribution predicted by FEM, Enikeev and Kruglov Model, and Ragab model for the dome formed after thirty-two 8-min cycles under the pressure of 250 kPa

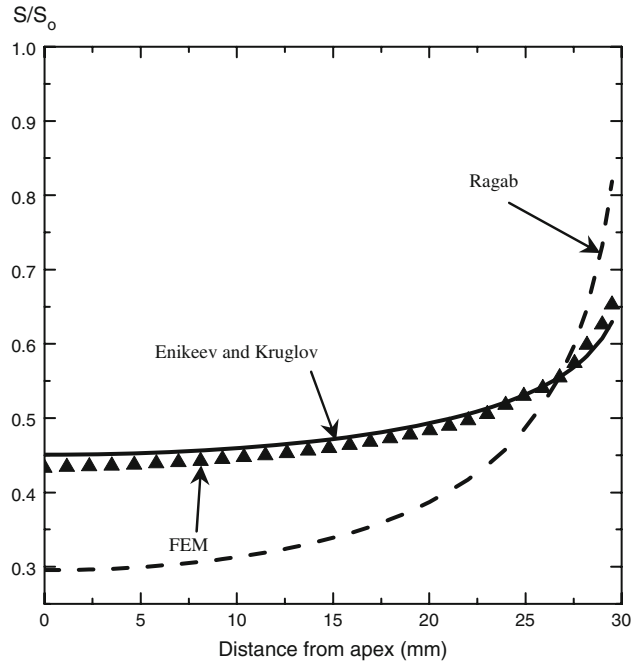

Fig. 8 The dome thickness distribution predicted by FEM, Enikeev and Kruglov Model, and Ragab model for the dome formed after ninety-eight 8-min cycles under the pressure of 200 kPa

that the stress in the dome should vary from the balanced biaxial state at the dome apex to the plane strain state at the dome edge, which is the assumption used for the Enikeev and Kruglov model; and it is not appropriate to assume a balanced biaxial stress state throughout the dome as in the Ragab model.

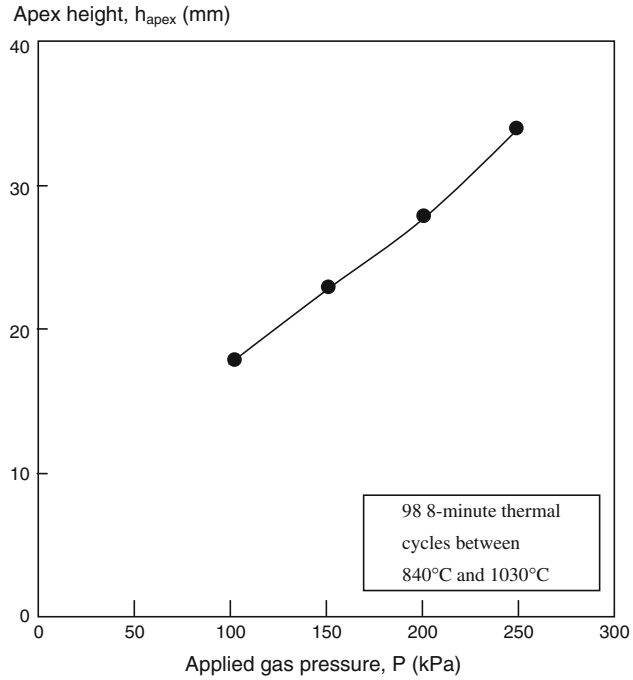

Fig. 9 The dome apex heights for different applied gas pressures through finite element modeling

3.4 Gas-Pressure Effect

Simulations with a series of different applied gas pressures were performed to study the effect of gas pressure on dome forming. Four gas pressures were used: 100, 150, 200, and 250 kPa. All of the simulations have the same forming time of ninety-eight 8-min cycles (784 min). Figure 9 provides the apex heights for the domes. The apex height increased linearly with the increase of the applied gas pressure.

4. Conclusion

The finite element method was used to study the transformation superplastic forming of domes from originally flat circular plate samples under applied gas pressure. The dome apex experienced the maximum stress and strain, while the stress and strain decreased when moving from the apex to the edge of the dome. During the dome test, the equivalent strain within the dome increased almost linearly with the forming time. For the formed domes, the apex had the thinnest thickness, the edge had the thickest thickness, and the thickness increased from the apex position to the edge position at all forming times. In the formed domes, the thickness distribution predicted from the modeling matches very well with the theoretical predictions based on the Enikeev and Kruglov model, while the predictions from the Ragab model deviate significantly from the modeling results. The comparison of the simulated and theoretical dome thickness distributions indicates that the stress in the dome should vary from the balanced biaxial state at the dome apex to the plane strain state at the dome edge. The apex height increased linearly with the increase of the applied gas pressure.

Acknowledgment

The support form University of Nevada, Reno is greatly appreciated.

References

1. T.G. Nieh, J. Wadsworth, and O.D. Sherby, *Superplasticity in Metals and Ceramics*, 1st ed., Cambridge University Press, 2005
2. M. Kawasaki, R.B. Figueiredo, C. Xu, and T.G. Langdon, Developing Superplastic Ductilities in Ultrafine-grained Metals, *Metall. Mater. Trans. A*, 2007, **38A**, p 1891–1898
3. M. Kawasaki and T.G. Langdon, Principles of Superplasticity in Ultrafine-grained Materials, *J. Mater. Sci.*, 2007, **42**, p 1782–1796
4. S.V. Dobatkin, E.N. Bastarache, G. Sakai, T. Fujita, Z. Horita, and T.G. Langdon, Grain Refinement and Superplastic Flow in an Aluminum Alloy Processed by High-pressure Torsion, *Mater. Sci. Eng. A*, 2005, **408**, p 141–146
5. C.Y. Gao, P. Lours, and G. Bernhart, Thermomechanical Stress Analysis of Superplastic Forming Tool, *J. Mater. Process. Technol.*, 2005, **169**, p 281–291
6. A. Dutta, I. Charit, L.B. Johannes, and R.S. Mishra, Deep Cup Forming by Superplastic Punch Stretching of Friction Stir Processed 7075 Al Alloy, *Mater. Sci. Eng. A*, 2005, **395**, p 173–179
7. C. Xu, M. Furukawa, Z. Horita, and T.G. Langdon, Developing a Superplastic Forming Capability in Nanometals, *Solid State Phenom.*, 2005, **101-102**, p 23–30
8. Y.T. Zhu and T.G. Langdon, The Fundamentals of Nanostructured Materials Processed by Severe Plastic Deformation, *JOM*, 2004, **56**, p 58–63
9. M. Kamachi, M. Furukawa, Z. Horita, and T.G. Langdon, Achieving Superplasticity of Al-1%Mg-0.2%Sc Alloy in Plate Samples Processed by Equal-channel Angular Pressing, *Mater. Trans.*, 2004, **45**, p 2521–2524
10. Y.T. Zhu, T.C. Lowe, and T.G. Langdon, Performance and Applications of Nanostructured Materials Produced by Severe Plastic Deformation, *Scripta Mater.*, 2004, **51**, p 825–830
11. V.N. Perevezentsev, V.N. Chuvil'deev, V.I. Kopylov, A.N. Sysoev, and T.G. Langdon, Developing High Strain Rate Superplasticity in Al-Mg-Sc-Zr Alloys Using Equal-channel Angular Pressing, *Ann. Chim.-Sci. Mater.*, 2002, **27**, p 99–109
12. A.V. Sergueeva, N.A. Mara, and A.K. Mukherjee, Plasticity at Really Diminished Length Scales, *Mater. Sci. Eng. A*, 2007, **463**, p 8–13
13. N.A. Mara, A.V. Sergueeva, T.D. Mara, S.X. McFadden, and A.K. Mukherjee, Superplasticity and Cooperative Grain Boundary Sliding in Nanocrystalline Ni3Al, *Mater. Sci. Eng. A*, 2007, **463**, p 238–244
14. R.Z. Valiev, A.V. Sergueeva, and A.K. Mukherjee, The Effect of Annealing on Tensile Deformation Behavior of Nanostructured SPD Titanium, *Scripta Mater.*, 2003, **49**, p 669–674
15. X. Zhang, H. Wang, R.O. Scattergood, J. Narayan, C.C. Koch, A.V. Sergueeva, and A.K. Mukherjee, Studies of Deformation Mechanisms in Ultra-fine-grained and Nanostructured Zn, *Acta Mater.*, 2002, **50**, p 4823–4830
16. G.W. Greenwood and R.H. Johnson, The Deformation of Metals Under Small Stresses During Phase Transformations, *Proc. Roy. Soc. Lond. A*, 1965, **283**, p 403–422
17. S.M. Pickard and B. Derby, The Influence of Microstructure on Internal-Stress Superplasticity in Polycrystalline Zinc, *Scripta Metall. Mater.*, 1991, **25**, p 467–472
18. B. Derby, The Mechanism of Internal Stress Superplasticity, in *Superplasticity in Metals, Ceramics and Intermetallics*, M.J. Mayo, M. Kobayashi, and J. Wadsworth, Eds., MRS, 1990
19. H. Zhang, G.S. Daehn, and R.H. Wagoner, Simulation of the Plastic Response of Whisker Reinforced Metal Matrix Composites Under Thermal Cycling Conditions, *Scripta Metall. Mater.*, 1991, **25**, p 2285–2290
20. D.C. Dunand and P. Zwigl, Hydrogen-Induced Internal-Stress Plasticity in Titanium, *Metall. Mater. Trans. A*, 2001, **32**, p 841–843
21. C. Schuh and D.C. Dunand, Internal Stress Plasticity due to Chemical Stresses, *Acta Mater.*, 2001, **49**, p 3387–3400
22. Q. Li, E. Chen, D. Bice, and D.C. Dunand, Transformation Superplasticity of Cast Titanium and Ti-6Al-4V, *Metall. Mater. Trans. A*, 2007, **38A**, p 44–53
23. M. Frary, C. Schuh, and D.C. Dunand, Kinetics of Biaxial Dome Formation by Transformation Superplasticity of Titanium Alloys and Composites, *Metall. Mater. Trans. A*, 2002, **33**, p 1669–1680
24. P. Villars, A. Prince, and H. Okamoto, *Handbook of Ternary Alloy Phase Diagrams*, ASM International, 1995
25. J.A. Ewing, *The Strength of Materials*, 2nd ed., University Press, 1906
26. R.T. Fenner, *Mechanics of Solids*, 1st ed., CRC, 1999
27. F.U. Enikeev and A.A. Kruglov, An Analysis of the Superplastic Forming of a Thin Circular Diaphragm, *Int. J. Mech. Sci.*, 1995, **37**, p 473–483
28. A.R. Ragab, Thermoforming of Superplastic Sheet in Shaped Dies, *Met. Technol.*, 1983, **10**, p 340–348